A Quasi-Spherical Net Power Fusion Reactor Based on High Temperature Superconducting Magnets

Joel G. Rogers (rogersjg@telus.net)
SAFEnergy Inc
Andrew A. Egly
SAFEnergy Inc
Frank J. Wessel
SAFEnergy Inc

Research Article

Keywords:

Posted Date: April 20th, 2023

DOI: https://doi.org/10.21203/rs.3.rs-2837895/v1

Abstract

Particle in Cell (PIC) simulation has been used to design a quasi-spherical, net power, deuterium fueled, fusion reactor incorporating high temperature superconducting (HTS) magnets. Using the principles of Magneto-Electrostatic Trap design of Yushmanov(1980) the reactor is predicted to have power-balance Q = 7, improving on the classic Polywell design by incorporating HTS magnets and a high-current deuteron ion beam. With these improvements, a hexahedral reactor of only 4m diameter is predicted to produce 100 megawatts of net power, in a design that is suitable for practical commercial fusion power production.

Introduction

This paper reports on the computer design of a net power fusion reactor constructed with six high-temperature-superconducting (HTS) magnets. Computer simulation results were analyzed using Yushmanov's magneto-electrostatic-trap (MET) theory [1]. Our six magnet design, which we named MET6, has a more efficient shape for plasma confinement than other recent MET designs. Yushmanov showed that optimum power-balance (Q) scales linearly with the volume-to-surface ratio of the confined plasma ball. For this reason our spherical design is expected to produce larger Q-values than recent cylindrical ones [2,3].

MET6 evolved naturally from its predecessor, the Polywell reactor, invented by Robert Bussard in 1989 [4]. Polywell suffered from a major flaw, first pointed out by Rider in 1994 [5] and then reinforced in the 2018 Jason Report summarizing the Department of Energy's ARPAE funding program [6]. The Jason Report stated that Polywell had been "conclusively ruled unworkable" and as a result Polywell research would not be considered for ARPAE funding. In rejecting Polywell, the Jason Report referenced Rider [5], claiming that Polywell's ions' nonthermal energy distribution would require too much energy to maintain and the device therefore could not reach unity power-balance.

The design of MET6 sidesteps this long-running controversy over Polywell's nonthermal energy distribution. In contrast to Polywell, the plasma in our simulation of MET6 has a Maxwellian energy distribution. In a real reactor a slight departure from Maxwellian distribution is known to occur in the extreme high energy tail of the distribution due to electrons up-scattering to energies exceeding the height of the trapping potential. This minor departure from Maxwellian distribution was ignored by Yushmanov [1], Dolan [2] and Sporer [3] and likewise in this paper. Pure Maxwellian energy distribution is used in analysis of our MET6 design.

Hardware Design – MET6 is a fusion reactor design comprised of six cylindrical, HTS coil-magnets mounted on the faces of a regular hexahedron (i.e. cube). Fig. 1 (a-c) shows diagnostic plots produced by a particle-in-cell (PIC) simulation program *OOPIC Pro*, licensed from Tech-X Corporation [7]. *OOPIC Pro* is no longer supported by Tech-X, but an equivalent public domain version of the software is available

from the University of Michigan under the name *XOOPIC*]8]. We compared XOOPIC with OOPIC Pro and found the results identical within statistical uncertainties.

Fig. 1(a) is a snapshot of an OOPIC Pro diagnostic showing a square outline with tick marks, the cross section of a cubic, metal vacuum tank. The tank serves as a grounded cathode emitting zero-energy electrons from a point source mounted on the inside of the right-hand tank wall. Inside the tank are shown eight square, metal magnet boxes containing HTS electromagnets' wire-windings. The magnet boxes are biased to 200kV from an external power supply, creating an anode attracting electrons from the point-source emitter. The combined effect of the bias voltage and the magnetic field from the wires is to collimate and accelerate electrons from the emitter into the center of the tank where they are trapped. Positions of 40K macro-particles are represented by 40K black dots. Each macro-particle is simulated to have the mass and charge of 4e9 real electrons. In the online version of Fig. 1(a), the dots representing electrons are seen to move randomly in and out from a central plasma ball along eight narrow cusp lines.

Although macroparticles are shown as zero-width dots in Figs. (a) and (c), the dots are treated as having internal structure when their charge is deposited on the grid of PIC cells. Macro-particles interact with each other electrostatically as if each were a cloud of charge [9]. At each time-step and for each macro-particle, a cloud of charge is divided among the 4 nearest cells, in proportion to the areas of 4 rectangles between the cloud-center and the cell-centers. Each cell accumulates charge from all particles near it. The electrostatic potential is computed by superposition of point particle electric fields originating from point charges located at the centers of each cell.

In the remainder of this paper macro-particles will be called by the appropriately shortened forms, "electron" and "ion."

After many passes in and out of the central ball, a typical electron gains enough energy by random up-scattering to overcome the anode's attracting voltage and hit one of the tank walls where it is lost. New electrons are continuously supplied by the emitter at an electrical current adjusted to just match the current of lost electrons. The reactor operates in steady state with electrons flowing continuously from the emitter to the central plasma ball, then out and in along cusp lines to finally be lost at the tank. Steady state is characterized by the density of electrons becoming constant in time. The snapshots of Fig. 1 were made after 1ms of electron injection and after adjusting the electron emitter's current to stabilize the density to a constant value.

The behavior of the plasma at later times of steady-state running was investigated using the public domain *XOOPIC* [8] software package, thought to be identical in function to the discontinued TechX commercial product. At the 1ms mark of plasma evolution the diagnostics from the public domain version agreed with the TechX commercial version, affirming that the public domain version can be used to provide a continuation of OOPIC Pro functionality, as described in the remainder of this paper. In addition to proving XOOPIC is equivalent to OOPIC Pro, XOOPIC was run for a longer time using the same input file as that producing Fig. 1.

The purpose of undertaking the extended-time analysis was to confirm that the plasma's velocity distribution had the Maxwellian shape predicted by Yushmanov [1] and assumed by Dolan [2], Sporer [3] and by us. A simulation run of 10ms was performed with the same input parameters used in the OOPIC Pro simulations of Fig. 1. The velocity distribution simulated at 1ms and 10ms were identical within statistical uncertainty. A Gaussian fit to the simulated electrons' and ions' velocity distributions indicated a plasma temperature of 30keV. This temperature is higher than the 11keV temperature predicted by our analysis following Yushmanov [1] as detailed in the next section of this paper. The lack of cooling between early time temperature and steady-state temperature can reasonably be attributed to a slow rate of actual thermalization compared to the 10ms of plasma evolution simulated with *XOOPIC*. Limited by available computing resources, the width of the Gaussian fit determining temperature is consistent with a Maxwellian distribution of gradually declining temperature.

The diagram of the reactor in Fig. 1(a) is a 2D section of the 3D reactor described in the text. Only the portions of the 3D reactor that intersect the central plane are shown. The magnet boxes shown outline two intersecting sections from each of four ring-magnets mounted on the four side-faces of a cube. The remaining two magnets of the six making a hexahedron are above and below the plane simulated, not intersecting the central plane. The magnetic and electric fields generated from these out-of-plane magnets sum to zero due to up-down reflection symmetry of the cube. The fields from the magnet located above the central plane exactly cancel the fields from an identical magnet located below the central plane. Including them in the simulation would not change the predicted diagnostics in the central plane; they were safely left out of the simulation.

Other polyhedral magnet layouts are possible to make other MET designs. Six magnets is the smallest number of magnets that can be arranged to produce a central symmetry plane required for ease of simulation. MET reactors with more than 6 magnets arranged on a higher-order polyhedron are an attractive idea for an advanced MET design [10]. The additional magnets would produce smoother bounding fields and therefore better confinement. However, simulating more magnets was not considered for this study due to the extra complexity of specifying them as input to the simulation package.

At each time-step the simulation program calculates the overall electrostatic potential by superposing the known point-source potentials from each PIC cell. Fig. 1(b) shows a snapshot of the 2D potential function resulting from this superposition. Although particles are in motion, the potential formed from the sum of all the individual potentials is constant in time as shown in (b). The maximum potential inside the tank is 200kV, which occurs in the 8 square areas inside the magnet boxes, colored magenta in the online publication of this article. Areas of minimum potential (0-20kV, shaded red online) exist at the center of the tank and near the tank walls. The ring of 8 magnet boxes form the rim of a potential-well effective for trapping ions

Fig. 1(e) shows a numerical graph of the potential voltage along the horizontal centerline of (b). Ions are continuously injected and travel initially along this line from an ion gun located on this line at the left-hand tank wall. Ions experience acceleration in proportion to the slope of this potential function. At first

newborn ions are decelerated by the rising slope of the left-hand barrier peak. The ion gun is tuned to produce ions of unique energy selected to just clear the potential barrier in the left-hand magnet. At the position of the maximum potential the newborn ions have been decelerated just enough that they enter the interior of the magnet enclosure with near-zero kinetic energy. The voltage equivalent of this unique energy, indicated by the dashed arrow, was found by trial and error to be 156kV. Newborn ions of this energy form into a beam, cross the center of the tank, reflect off the potential barrier in the right-hand magnet, and return toward the center to become trapped in the 20kV-minimum potential-well.

Fig. 1(c) shows 10K dots representing the ions' positions at steady state. The areal density of ions in (c) is seen to be approximately the same as the electrons in (a). Matching densities of ions and electrons was done by trial and error adjustment of the current from the ion gun. The steady-state value of ions' injection current was found to be much smaller than the electrons' emitter-current. The electrons insulate average-energy ions from hitting the tank.

In addition to the electrons injected from the emitter, electrons are also injected from an electron gun on the left-hand tank wall at the same position as the ion gun. These electrons are matched in velocity and current with the ions' velocity and current for the purpose of neutralizing the space charge of the ion beam at the point of its injection. The design of this neutralized ion beam source was originally proposed by Wessel et al. [10] for cross-field injection into magnetically confined plasma and more recently adapted for fueling a newly proposed spherical fusion reactor [11]. In Fig. 2(a) the ion plus electron sources are marked by a short vertical (orange online) bar at the center of the left-hand wall. The height of the bar measures 2 PIC cells, approximately the same as the 17cm high beam described in Ref. [11].The simulation tracked these neutralizing electrons separately from the electrons from the main emitter on the right-hand tank wall. These neutralizing electrons become trapped in a distribution identical to the electrons in Fig. 1(a). Being much lower in number than the electrons from the main emitter, and having the same spatial distribution, the neutralizing electrons could be safely ignored in estimating the power-balance.

An extra electrode is shown at the head of the arrow in Fig. 1(a). This electrode forms a narrow opening called an "anode gap" [1]. The anode gap raises the potential barrier at its position to be higher than the potential barrier where newborn ions enter through the left-hand magnet. The higher barrier prevents newborn ions from escaping to the right at the position of the dashed-arrow head in Fig. 1(e). The anode-gap also has an important function when the density rises to net power values. It plays a role in pumping out cold electrons which otherwise form a space charge blocking the free passage of electrons from the electron emitter. This role is discussed in more detail below in reference to Fig. 2, which shows reactor diagnostics made at net-power plasma densities.

Fig. 1(f) shows the ions' coordinates in velocity-position space. In the online display of this diagnostic, ions from the ion gun are seen moving to the right at the head of the downward-pointing arrow. These ions cross the tank from left to right, reflect from the barrier on the right, and return to the left-hand barrier where a small fraction of them, indicated by the upward-pointing arrow, return to the left-hand tank wall to

be lost. Having little chance to fuse, these lost ions waste the power used to create them in the ion gun. This wasted power exists only in diagnostics made at early time during startup. As the trapped plasma density is raised toward net-power value, the amount of energy lost by newborn ions returning across the center to the right-hand barrier increases. At higher densities the energy retained by the newborn ions on their return through center is less than the height of the left-hand barrier. In this case a negligible current of newborn ions will escape back along the path pointed to by the upward-pointing arrow. During these later phases of startup the current of ions from the ion gun will all be trapped to raise the plasma's ion density to net-power level with ions' injection current very small compared to the electrons' current.

At steady-state net-power operation, a steady flow of ions will continually escape along all 8 cusp lines due to up-scattering in energy (i.e. thermalization). Escaping ions are barely noticeable at the low-density operation illustrated in Fig. 1. Of 10K ion particles plotted in (c) and (f), only one ion particle, pointed to by the left-pointing arrows, is seen to escape through the right-hand barrier. That such a small fraction of ions escape over the barrier is a measure of the efficiency of insulation provided by the electrons to conserve the ions.

The magnetic field in the simulation was modeled as if produced by the electrical current in eight straight wires, oriented perpendicularly to the simulation plane and located at the centers of the eight magnet boxes shown in (a) and (c). The fields from 8 infinite straight wires were calculated from a textbook formula and summed at each cell and stored to form two 50x50 arrays, one array for x-components and one for y-components. The hexahedron's 3D magnetic field is more complex than the 2D simulated field. Fig. 1(d) is a cartoon of a surface of constant field-magnitude [12]. A total of 26 cusp-openings penetrate the surface, 6 face-cusps, 8 corner- cusps, and 12 edge-cusps. The central plane is shown outlined by a rectangle of dashed and solid lines. This plane contains 8 cusps, typical ones indicated by arrows; two horizontal arrows point to 2 typical face-cusps and a vertical arrow points to a typical edge-cusp. In the simulation, strong magnetic fields along the cusp lines squeezes the recirculating electrons into 8 narrow beams, each beam of width approximately half the width of a PIC cell.

Our use of a high intensity particle beam for fueling MET6 is a major improvement over Polywell designs fueled by internal deuterium gas-cells [13]. The vacuum system for MET6 is required only to pump away out-gassing; it is no longer required to pump away the much higher load of neutral fuel gas leaking from the internal gas-cell [13]. In parallel work, high-intensity negative-deuteron ion sources are being developed as the first stage of neutral beam generation for ITER [14]; these D sources may be adapted for MET6 as a possible improvement on the Wessel design [10].

The diagnostic plots in Fig. 1 are from simulating a reactor operating at the minimum plasma density producing good electron confinement. The plasma density required for net power is many orders of magnitude higher than this minimum density [15]. Without changing the hardware configuration the density can be raised by raising the injection current of electrons and ions. To investigate the scaling of density with injection currents, a new simulation was run with these currents raised by a factor of two from the values in Fig. 1. As expected, the steady-state densities also rose by the same factor. A direct

way to simulate net power would be to continue to increase the simulated injection currents step-by-step until diamagnetic effects expand the plasma ball and the density becomes limited by the β=1 condition just inside the ring of magnets. In simulation, such a direct approach proved impractical due to the need to match electron and ion densities to a high degree of precision, as required to maintain the plasma's quasi-neutrality.

Diamagnetic expansion has been demonstrated to actually occur by Lavrentev, who also associated the expansion with the appearance of a central "volume of superseded magnetic field" [16]. "Superseded magnetic field" is caused by the plasma's natural tendency to generate internal currents that cancel the applied magnetic field throughout the plasma's volume. For speed of execution we ran the OOPIC code in "electrostatic mode." In this mode the magnetic field is static and derived from the DC currents in the 8 wires. An alternate technique to produce a superseded volume was invented to circumvent this restriction of the electrostatic PIC code.

Fig. 2 shows diagnostics from a separate simulation run to investigate the reactor's performance when the plasma density is raised to net-power levels. Comparing Fig. 1(a) with Fig. 2(a) shows that the volume of the plasma is much bigger in Fig. 2. As an approximate work-around for a rigorous simulation of diamagnetic effects, the applied magnetic field was modified by replacing the computed-field by zero-field, cell-by-cell, in all cells inside a square region at the center of the tank. Fig. 2(d) shows the x-component of the magnetic field, Bx, which was available as a standard diagnostic from the simulation. A square-shaped region of zero fields is labeled "0T" at the center of the panel. The diameter of the zero-field-region was adjusted by trial and error to make the diameter of the recirculating electron-beam just fill the anode gap, shown at the head of the vertical arrow in (a). Just filling the gap allowed a small portion of the recirculating electrons to be scraped off on the edges of the gap. This scraping was found to produce a beneficial effect of reducing the density of space charge build-up in the cusps.

Understanding the behavior of the recirculating electron beam as it passes back and forth through the anode gap is crucial to the design of any MET reactor. Optimizing the geometric shape of hypothetical anode gaps to increase the power-balance Q is the subject of a second Yushmanov study [17]. Yushmanov only considered a rectangular gap, parameterized by width and depth. The gap shown in Fig. 2 models a more complex gap shape, consisting of the cylindrical magnet's bore partially closed by a thin metal disc with a circular hole drilled in it. In the simulation the fields in the gap depend on three parameters, namely the inside diameter of the magnet, the diameter of the hole, and the thickness of the magnet along the horizontal direction. The shape of the gap simulated was chosen for simplicity in specifying it in the language dictated by the conventions of the OOPIC software. No attempt was made to vary the shape to increase the power-balance.

Previous MET simulations [18] had also shown that adjusting the gap to intercept a percentage of circulating electrons would reduce the undesirable accumulation of space-charge in the anode cusps. In this sense, the gap serves to pump out the low energy electrons that tend to accumulate in the bores of the magnets. In the simulation of Fig. 2, the minimum amount of electron current hitting in the gap was

found from a diagnostic to be 4% of the injected electrons' current. This current was made as small as possible to minimize the power taken away by the lost electrons. Pumping out of electrons to reduce the space-charge imposes a performance cost by consuming some of the drive power which is the denominator of Q.

The size of the anode gap was taken to be 2 PIC cells, the smallest non-zero size permitted by the software. The number of cells filling the central plane was chosen as 50x50, minimized to keep the computer time to simulate approximately 50h per run. Spanning the 4.12m diameter of the tank with 50 cells, one PIC cell therefore measured 4.12m/50 = 8cm. With this choice of anode gap, 2 cells measured 16 cm. This choice dictated the other parameters of the simulated reactor. The diameter of the field-free region was optimized to be 75% of the distance between the interior faces of the magnet coils. The recirculating electron beams spread out in crossing the zero-field region. The diameter of the field-free region determined the diameter of the beam passing in and out through the anode gap. Maximum plasma diameter is desired to maximize plasma volume, and thereby the fusion power which is the numerator of Q.

Estimating the Power-balance Q from the PIC Diagnostics – Yushmanov [1] derived a general expression for the optimum power-balance Q_{max} for a hypothetical toroidal multi-cusp reactor burning DT fuel. The derivation was general enough to apply to other reactor geometries and other fuels. For example, Dolan-1994 and Sporer-2022 have used Yushmanov's results to analyze performance of a linear multi-cusp reactor. Here we apply Yushmanov's analysis to our hexahedral MET6 reactor. From Yushmanov's equation (10) we will evaluate the following expression for power-balance:

$$Q_{DT} = 4\,(U-\Delta U)^{3/2}\, n^{1/2}\, b\, a\, B, \qquad (1)$$

where U is the applied magnet-bias voltage [in units of100kV], ΔU is the depression of the confining potential due to space charge [in units of 100kV], n is the ion density [in units of 1e14/cc], b is the anode gap half-width [in units of mm], a is the volume-to-surface ratio of the plasma ball [in units of m], and B is the magnetic field at the anode [in units of 100kG = 10T]. The numbers in brackets in the just-stated list specify units which were created by Yushmanov to make the factors contributing to Q have numerical values near unity. For example, our 200kV bias would be expressed as U=2 in Yushmanov's units.

On the left-hand side of eq. (1) we have added a "DT" subscript to Yushmanov's Q symbol to remind us that Yushmanov assumed DT fuel in deriving his power-balance ratio. Eq. (1) contains the reactivity and energy yield of the DT reaction absorbed into its right-hand side's leading numerical factor. In the following we first compute the power-balance we would expect if our MET6 hardware were fueled with deuterium plus tritium. Then we convert the resulting Q_{DT} value to Q_{DD} by multiplying Q_{DT} by the known ratio of DD to DT reactivity times energy gain.

In eq. (1), the factor U-ΔU comes from Fig. 2(e). The shape of the potential curve in 2(e) is somewhat different from the symmetric shape assumed by Yushmanov in his “FIG. 1.” Our placement of the anode gap electrode in the right-hand magnet creates an asymmetric potential shape not present with Yushmanov; our right-hand peak is taller than the left-hand peak. This asymmetric confining potential was essential to facilitate the trial and error adjustment of the incoming ions’ energy in the early phase of startup. To adapt our PIC result to Yushmanov’s formula we naturally assigned the average ΔU=20kV, making the average U-ΔU, shown by the dashed arrow in (e), to be 180kV. Converting 180kV to the units shown in brackets above yields the following assignment of the potential factor in eq. (1):

U-ΔU = 1.8.

The next factor in Q_{DT} is the ion density “n.” This was determined by inverting the β=1 equation, which defines the surface of the plasma ball. From pg. 29 of the Plasma Formulary, inverting the β=1 equation results in the following expression for electron density:

$$n = B_s^2 / [(4e\text{-}11)\ T], \qquad (2)$$

where B_s is the magnitude of the magnetic field vector at the surface of the plasma ball and T the electron-energy, both expressed in cgs units. A convenient point on the surface of the plasma ball was chosen for graphical determination of B_s. The double-headed arrow in (a) marks 2 surface points where the x-component of the magnetic field Bx is zero, leaving B_s equal to its y-component, By. Fig. 2(f) shows a graph of simulated By, plotted as a function of x-coordinate along the path of the double-headed arrow in (a). The value of By at the surface is marked by the arrow in (f), placed to indicate the value of B_s just outside the bounding sheath of the plasma ball. On the vertical scale the arrow points to By = B_s = 7 teslas = 70 kilogauss in cgs units as required in eq. (2). The remaining factor in eq. (2) is the electron energy T. Yushmanov found by “numerical calculations” that “plasma temperatures amount to 1/16 of the energy e(U-ΔU).” The dashed arrow in Fig. 2(e) shows e(U-ΔU) equals to 180keV, making T =180keV/16 = 11keV. Inserting these values of B_s and T into eq. (2) gives the following for electron density, assumed equal to ions’ density as a result of the central plasma’s quasi-neutrality:

$n = (70e3)^2 / [(4e\text{-}11)\ (11e3)] = 1.11e16\ /cm^3 = 111$ using the bracketed units from eq. (1).

The next factor to determine Q_{DT} in eq. (1) is “b”, the half-width of the anode gap. As described in the final paragraph of the previous section of this paper, b is made equal to one PIC cell-width. From the chosen tank diameter divided by the chosen number of PIC cells spanning the tank,

b = 1 PIC cell-width = 4.12m/50 = 8cm = 80 in the bracketed units.

The next factor is “a”, the ratio of the volume of the plasma ball to the surface area of the plasma ball. This factor depends on the shape of the plasma ball. From the shape shown in Fig. 1(d), the central ball, excluding the cusps, is approximately a cube. A cube has volume-to-surface ratio of its diameter divided

by 6. Fig. 2(c) shows the ion density along the line shown by the double-headed arrow in Fig. 2(a). The base width of the ion's plasma ball is 1.9m. The volume-to-surface ratio is therefore:

a = 1.9m/6 = 0.32m = 0.32 in the bracketed units for the volume-to-surface ratio.

The final factor in Q_{DT} is the magnitude "B" of the magnetic field vector at the position of the anode gap. From Fig. 2(d) B = 18T = 180 kilogauss.

B = 180 kilogauss = 1.8 in the bracketed units for anode B field.

Collecting the five factors required to evaluate the expression in eq. (1),

$Q_{DT} = 4\ (1.8)^{3/2}\ (111)^{1/2}\ (80)\ (0.32)\ (1.8) = 4\ (2.4)\ (10.5)\ (80)\ (0.32)\ (1.8) = 4.6e3.$

The final step in estimating the power-balance of our DD fueled reactor is to convert the above estimate of Q_{DT} to an estimate Q_{DD}, the power-balance resulting when DT fuel is switched to DD. The power-balance from Yushmanov's eq. (10) for Q_{DT} contains a factor $\langle v\sigma_{fus}\rangle_{DT}E_{DT}$, the product of averaged fusion reactivity times the energy released by each DT fusion event. We can convert the Q_{DT} expression to the equivalent expression for DD fusion by multiplying Q_{DT} by the ratio of cross sections times the ratio of fusion energies. From the pg. 45 of the Plasma Formulary the ratio of DD to DT reactivity is $\langle v\sigma_{fus}\rangle_{DD} / \langle v\sigma_{fus}\rangle_{DT}$ = 1.2e-19 / 1.1e-17 = 0.0109. The second factor, the ratio of fusion energies, is E_{DD} / E_{DT} = 2.5MeV / 17.6MeV = 0.142. The numerator E_{DD} is the energy of the charged particles, excluding the neutrons' energy. In the denominator the 17.6 MeV must include the neutrons' energy because the bulk of the DT reaction's energy resides with the neutron; it must be captured. Applying these two factors to the DT power-balance estimated above gives the following expression for the power-balance of our 4.12m DD reactor:

$Q_{DD} = (Q_{DT})\ (.0109)\ (0.142) = (4.6e3)\ (1.5e\text{-}3) = 7$

While less than the hoped for Q=10, this power-balance is enough in excess of unity to make the MET6 reactor a possible contender for the fusion world's preferred net-power reactor design.

Calculating P_{fusion} from PIC Diagnostic Graphs – The fusion power output P_{fusion} was computed graphically from the displays produced by the PIC simulation program, shown in Fig.2. The standard textbook formula [19] for fusion power from fusing DD plasma is:

$$P_{fusion} = \tfrac{1}{2}\, n^2 \langle\sigma v\rangle\, E_{DD}\, V, \qquad (3)$$

where n is the deuterons' particle density, $\langle\sigma v\rangle$ is DD reactivity averaged over a Maxwellian energy distribution at T=11keV temperature, E_{DD} is the average energy released by fusing DD pairs, V is the ion cloud's volume. The first factor was determined in the previous section to be n = 1.11e16 cm^{-3}. The second and third factors, from the Plasma Formulary are $\langle\sigma v\rangle$ = 1.6e-18 cm^3/s and E_{DD} = 2.5MeV. The

final factor, the volume of the ion plasma ball, was taken to be the volume of a cube of dimension equal to the width of the ball at the position of the double-headed arrow in Fig. 2(a). From Fig. 2(c) this size is 1.9m, which gives a volume V = $(190cm)^3$ = 6.9e6 cm^3. Substituting these values into eq. (3) gives the following value for the fusion output power of the reactor:

P_{fusion} = 0.5 $(1.11e16)^2$ (1.6e-18) (2.5e6) (6.9e6) eV/s = 1.7e27 eV/s = 270 megawatts.

This is the power delivered as kinetic energy to the charged reaction products. The 2.45MeV neutron is allowed to escape. Charged particles will be magnetically steered to hit the tank walls along cusp lines. Conversion to electricity may be done at the tank wall, either by a turbine operating the Rankine cycle or by direct conversion using an electrical grid [20]. In converting to electricity the useful level of power will be further reduced by the efficiency of the energy conversion device used to convert kinetic energy into electricity. This efficiency can be assumed to be in the range 0.3 to 0.6, depending on whether the conversion to electricity is by a turbine or by direct conversion. Taking this range of efficiencies as equivalent to a relative uncertainty in electrical power, it is safe to say a conservative estimate of useable output power to the grid is 100 megawatts. This is surprisingly the same power output Sporer estimated from his linear-set-of-ring-cusps design with HTS magnets.

Discussion Of Results

A reliable PIC simulation has been coupled to the classic MET analysis method of Yushmanov [1] to design a compact, quasi-spherical reactor. Table 1 shows the final simulation parameters of MET6 compared to Sporer's cylindrical design [3].

Table 1 – Comparison of Sporer's HTS reactor with our MET6 reactor

Reactor Parameter	Sporer's HTS	MET6
B-field in anode cusps B (Teslas)	16	18
Applied voltage U (kV)	500	200
Anode gap spacing b (mm)	4	80
Plasma electron density n (m^{-3})	2.9e20	1.11e22
Plasma temperature T (keV)	25	11
Coil/cusp radius R (cm)	83	57
Plasma length L (m)	10	4.12

Fuel species	D+tritium	D+D
Gain Q	10	7

The bottom line of the table shows that the two reactor designs have similar gain factors, the main metric for performance. The most important advantage of MET6 over Sporer's design is shown in the penultimate line of the table. MET6 burns pure deuterium fuel, available virtually for free from seawater. Sporer's design, like most of the many tokamak designs (ITER, SPARC, EAST, etc.), would burn tritium, scarcely available on Earth from a few aging Candu reactors [21].

As the plasma density rises during startup, electrons' space charge accumulates in the cusps unless suppressed by some active means. Unless suppressed, the accumulation of space charge would be a fatal effect leading to the loss of the potential-well due to the reduced energy of incoming electrons after plowing through the trapped charge. A major discovery of this work is that scraping the exterior surface of the bounding sheath can eliminate the loss of the potential-well. Suppression of the space charge trapped in the cusps required a minimum of 4% of the incoming electrons' current be lost by hitting the gap-confining aperture. The surface layer of the sheath was scraped off by the edges of the aperture. This scraping halted the build-up of trapped electrons, in effect pumping out low energy electrons from the cusp traps. If any less than 4% of injected electrons hit the gap aperture, the trapped electrons' density increased without limit, resulting in the loss of the essential potential-well after a few milliseconds of operation.

The amount of power required for scraping depends on the detailed structure of the plasma inside the thin sheath marking the boundary between field-free interior and plasma-free exterior to the central ball of plasma. The details of the internal structure of the sheath are blurred by our choice of PIC cell size much larger than the electron gyro-radius. An improved PIC technique is reported by Park et al. [22]. The Park article reports PIC simulation investigating the relationship between PIC cell size and sheath structure in simulating a picket-fence plasma device. The article demonstrates that resolving the detailed structure of the simulated sheath requires choosing the PIC cell size to be small enough to resolve the electron gyro-radius in the sheath. Simulating with such fine-cell resolution required approximately 100,000 hours of processor time for each simulation run. The relevance of the Park et al. simulation to our MET reactor design is only indirect, since their picket-fence device lacked grid bias, an essential feature if the device were to function as a plasma trap.

On the contrary, the simulation runs reported in this paper required a more modest 50h of 3.2GHz processor time but failed to resolve the interior structure of the sheath. In our design the confined ions are insulated from the sheath by the potential-well of the trapped electrons. The estimated power-balance of Q=7 does not depend on details of sheath structure, because the 4% power lost to the aperture is small enough to be ignored in computing Q.

To see if our conclusions depend on PIC cell size, a separate simulation run was made with the same parameters shown in Table 1 but with PIC cell size ½ the cell-size used to produce Figs. 1 and 2. The higher-resolution simulation produced the same confining potential-well (U-ΔU) and ion density n, as the lower-resolution simulation. From eq. (1), simulation with these factors held constant will have the same power-balance as predicted for the lower resolution. This check shows that with even modest computing power it is possible to make a reliable estimate of power-balance, as long as the power lost to the aperture is kept small compared to the total injected power.

Conclusions

Particle in Cell (PIC) simulation has been used to design a quasi-spherical, net-power, deuterium fueled, fusion reactor incorporating high temperature superconducting (HTS) magnets. The reactor is predicted to have power-balance Q = 7, making the design suitable for practical commercial fusion power production.

Declarations

Acknowledgment – The authors thank Brendan Sporer for valuable discussions and critique of the manuscript.

References

1. E.E. Yushmanov, *The power gain factor Q of an ideal magneto-electrostatic fusion reactor*, Nucl. Fusion **20** 3 (1980)
2. T.J. Dolan, *Magnetic electrostatic plasma confinement*, Plasma Phys. Control. Fusion **3**, 1539 (1994)
3. B.J. Sporer, *Analysis of Two Fusion Reactor Designs Based on Magnetic Electrostatic Plasma Confinement,* J. Fusion Energ **41** 5 (2022)
4. R.W. Bussard, *Method and apparatus for controlling charged particles*, US patent 4826646 (1989)
5. T.H. Rider, *Fundamental limitations on plasma fusion systems not in thermodynamic equilibrium*, Physics of Plasmas**4**, 1039 (1997)
6. JASON The MITRE Corporation, *Prospects for Low Cost Fusion Development,* report JSR-18-01 (2018)
7. *OOPIC Pro* licensed from Tech-X Corporation, Boulder, Colorado, USA (2016)
8. Prof. J.P. Verboncoeur, *XOOPIC* The Plasma Theory and Simulation Group, http://ptsg.egr.msu.edu/ (2023)
9. Prof. C.K. Birdsall, *Particle-in-Cell Charged-Particle Simulations Plus MonteCarlo Collisions with Neutral Atoms, PIC-MCC*, IEEE Transactions on Plasma Science, **19** 2 (1991)
10. F.J. Wessel, J.J. Song, H.U. Rahmana), G. Yur, N. Rostoker, and R.S. Whitea, *Propagation of Neutralized Plasma Beams*, Physics of Fluids B: Plasma Physics, **2** 6 (1990)

11. F.J. Wessel, *PLASMA CONFINEMENT APPARATUS FOR NUCLEAR FUSION*, US patent application 2022/0359093 (filed May 5, 2022)
12. M. Carr, D. Gummersall, S. Cornish, and J. Khachan, *Low beta confinement in a Polywell modeled with conventional point cusp theories* "Fig. 12," Physics of Plasmas **18** 11 (2011)
13. J.G. Rogers, *APPARATUS AND METHOD FOR CONTROLLING A PLASMA FUSION REACTOR*, US patent 10204709 (2016)
14. M. Bacal and M. Wada, *Negative ion source operation with deuterium*, *Plasma Sources Sci. Technol.* **29** 3 (2020)
15. Scott Cornish*, A study of scaling physics in a Polywell device*, Pg. 15,Ph.D. thesis, Univ. of Sydney (2016)
16. O.A. Lavrent'ev, V.A. Maslov, , M.G. Nozdrachov, V.P. Oboznyj, S.A. Golyuk, N.A. Krutko, *MULTISLIT ELECTROMAGNETIC TRAP "JUPITER 2M3"*, Problems of Atomic Science and Technology **1** Series: Plasma Physics **13** 27 (2007)
17. E.E. Yushmanov, *THE INFLUENCE OF ELECTRON CAPTURE IN GAPS ON THE EFFICIENCY OF THE MAGNETO-ELECTROSTATIC TRAP*, Nuclear Fusion, **21** 3 (1981)
18. J.G. Rogers, *A Polywell Fusion Reactor Designed for Net Power Generation*, J. Fusion Energ **3** 1 (2018)
19. Samuel Glasstone and Ralph R. Lovberg, *Controlled Thermonuclear Reactions, an Introduction to Theory and Experiment*, eq. 2.9, D. van Nostrand Company, Inc., Princeton, New Jersey (1960)
20. W. Greatbatch, *^{3}He Fusion with Direct Electrical Conversion*, US patent 8059779 (2011)
21. Daniel Clery, *Out of gas. A shortage of tritium fuel may leave fusion energy with an empty tank, Science **376** 6600* (2022)
22. J. Park, G. Lapenta, D. Gonzalez-Herrero and N. Krall, *Discovery of an Electron Gyroradius Scale Current Layer: Its Relevance to Magnetic Fusion Energy, Earth's Magnetosphere and Sunspots,* Frontiers in Astronomy and Space Sciences **6** 74 (2019)

Figures

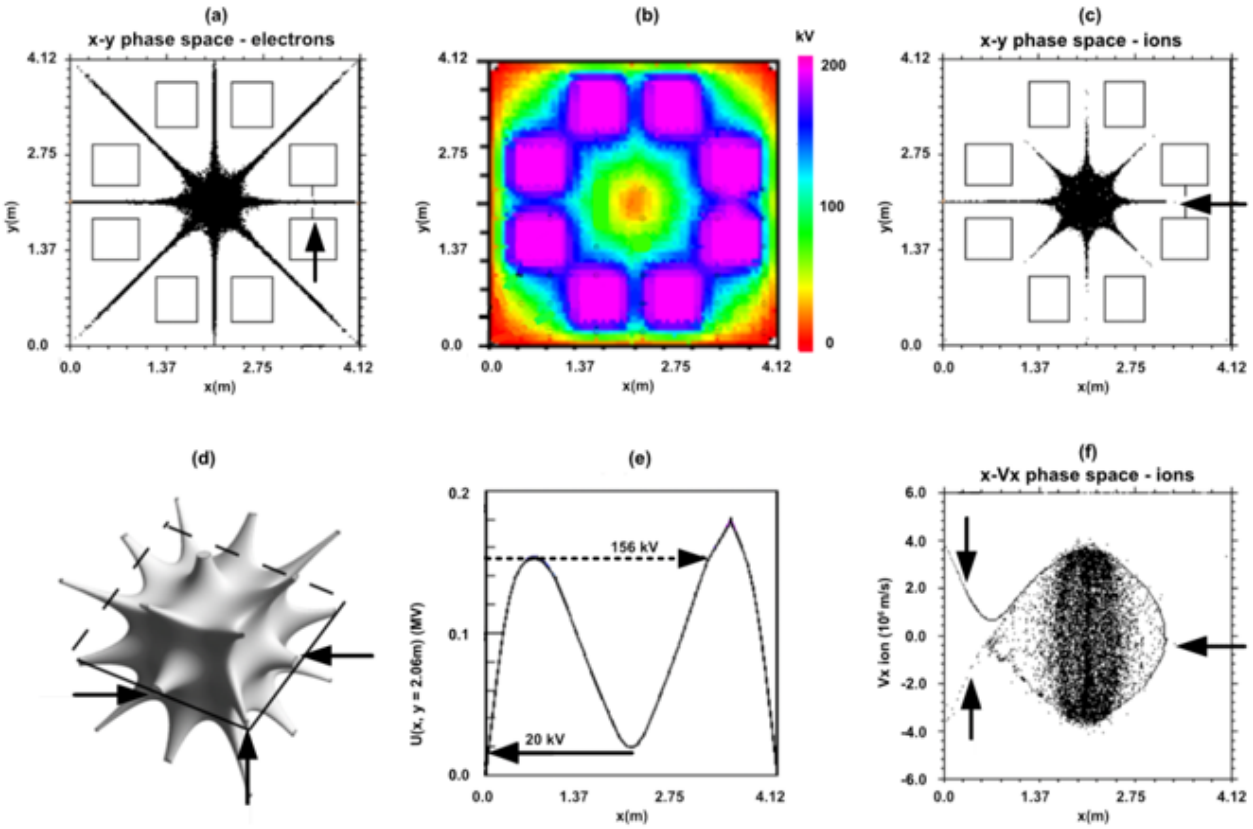

Figure 1

Snapshots of PIC diagnostic-displays from simulating an MET6 fusion reactor operating in low-density mode. Individual panels are as follows: a 2D positions of macro-electrons originating from the right-hand source. b 2D electrostatic potential function color-coded. c 2D positions of macro-ions originating from the left-hand (ion) source. d Iso-field magnetic surface at arbitrary magnetic-field magnitude. e 1D horizontal-central-section of above 2D function. f Macro-ions' positions in x-velocity vs. x-position space.

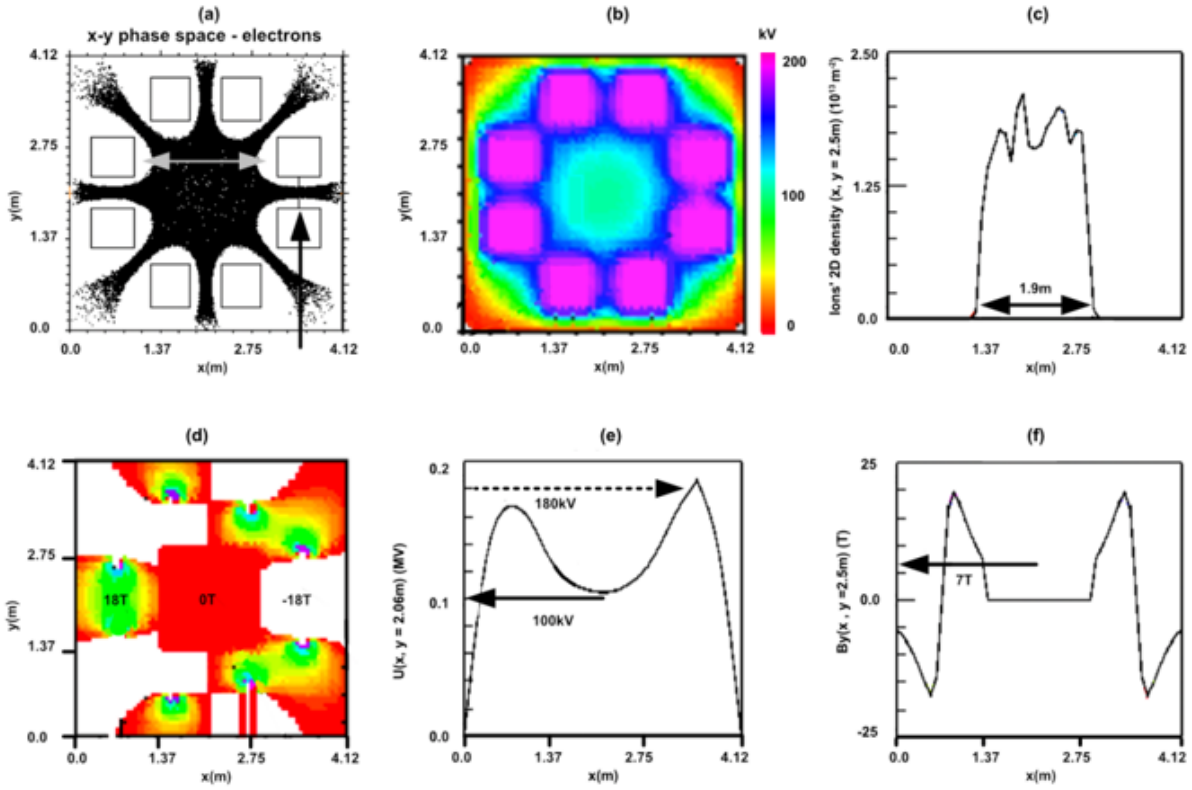

Figure 2

Snapshots of PIC diagnostic-displays from simulating an MET6 fusion reactor operating in β=1 high-density mode. Individual panels are as follows: a2D positions of macro-electrons originating from the right-hand (electron) source. b 2D electrostatic potential function color-coded. c 1D section of ion density at position of double-arrow in (a). d 2D x-component of magnetic field Bx color-coded (online red codes zero magnitude). e 1D horizontal-central-section of above 2D potential function. f 1D section of y-component of magnetic field By, the section made along the path indicated by the double-arrow in (a).